Final-state effects in neutron scattering from liquid neon

M. A. Fradkin,* S.-X. Zeng, and R. O. Simmons
Frederick Seitz Materials Research Laboratory and Physics Department, University of Illinois at Urbana-Champaign, Urbana, Illinois 61801-3080
(Received 30 December 1993)

We report inelastic scattering measurements of the neutron Compton profile, $J(y)$, in liquid Ne, over a broad range of neutron wave-vector transfers for liquid at a density of 36.1 atoms nm^{-3} at 27 K. The measurements used a chopper spectrometer at a pulsed-spallation neutron source. The wave vectors span the range 105 to 276 nm^{-1}, a range in which deviations from impulse-approximation scattering are expected to be dominated by final-state effects. Spectrometer resolution and sample-dependent multiple scattering were taken into account using a sophisticated Monte Carlo simulation. The data were analyzed, using the series expansion of Sears, to determine the magnitude of the first antisymmetric term in the expansion as a function of wave-vector transfer. Special care was taken to assess possible contributions arising from systematic errors. We find that the measurements agree very well with a calculation using a pair-distribution function, $g(r)$, from path-integral Monte Carlo simulation of liquid Ne near this density and temperature.

I. INTRODUCTION

The momentum distribution of atoms in a liquid or solid can be directly determined via inelastic neutron scattering if the momentum transferred to the target atom by the neutron in the scattering process is large enough. This is because at large momentum transfers, $\hbar Q$, the scattering has the form of scattering from a noninteracting gas of particles having the same momentum distribution as the actual target atoms. Such deep-inelastic neutron scattering has been used to measure momentum distributions in solid[1,2] and liquid[3,4] He, the other noble gases in solid and liquid phases,[5–7] liquid and solid H_2,[8] hydrogen embedded in a host matrix,[9] hydrogen bonds,[10] pyrolytic graphite,[11] as well as simple metals.[12] Unfortunately, experimental circumstances, such as low neutron flux and poor instrument resolution at large incident neutron energies, forced early experimenters to conduct such measurements in a regime where the impulse approximation (IA) is not strictly valid. Because of this, deviations from the IA due to final-state effects in the neutron scattering have been the subject of a great deal of interest.[13] In this paper we examine the form of these deviations in liquid Ne.[14]

Much of the early neutron inelastic-scattering work on liquid Ne focused on examination of collective excitations.[15] Single-particle neutron-scattering measurements performed on liquid Ne were those of Buyers *et al.*[16] In these experiments the dynamic scattering factor, $S(Q,\omega)$, of liquid Ne at 26.9 K was examined for 34 values of Q, in the range 8–125 nm^{-1}. Analysis of these data indicates that in liquid Ne, collective behavior is probed when Q is less than approximately 40 nm^{-1}, while the scattering for larger Q becomes characteristic of single-particle response, that is, (i) the peak position follows the recoil energy

$$\hbar\omega_R = \frac{\hbar^2 Q^2}{2M} , \tag{1}$$

where M is the mass of the target atom, and (ii) the width of $S(Q,\omega)$ increases linearly with Q. Buyers *et al.* observed oscillations in both the width and peak position of $S(Q,\omega)$ for Q less than approximately 100 nm^{-1}. These oscillations are attributable to interatomic interference effects, and their presence indicates that the IA is not valid. Final-state effects are also present in these data, but it is not possible to determine their contribution explicitly. The scattering data for $50 < Q < 100$ nm^{-1} were later reanalyzed by Sears to obtain a value for the kinetic energy.[5] He used a symmetrization procedure to remove the effect of final-state interactions and averaged the scattering function over a range of wave-vector transfers to remove coherent contributions.

With the advent of pulsed-spallation neutron sources, scattering experiments at wave-vector transfers larger than those easily accessible at reactor-based neutron sources became possible. Peek *et al.*[7] measured the scattering function $S(Q,\phi)$, where ϕ is the scattering angle, in liquid Ne at several sample densities and temperatures, in the range 200 $nm^{-1} < Q < 280$ nm^{-1}. At these large values of Q, interatomic interference effects are negligible and distortions due to final-state effects are expected to be small compared to unaccounted for multiple-scattering backgrounds and statistical uncertainties.

With improvements in the understanding of instrument resolution and multiple-scattering corrections as well as the increase in neutron flux brought about by high-current accelerators and improved spallation-target designs, high-quality data at both large and small Q can be obtained in which final-state effects must be accurately taken into account for correct interpretation. A number of theories have been developed for calculating the form of final-state effects. Unfortunately the complex calculations associated with several of these theories have only been performed for He.[17,18] However, a treatment of final-state effects due to Sears[19] is applicable to a wide variety of systems.

0163-1829/94/49(22)/15563(10)/$06.00

Liquid Ne is an excellent system for investigating the applicability of Sears' theory because (i) good quality low-Q data exist for liquid Ne which indicate interatomic interference effects are small at Q values greater than 100 nm^{-1}, therefore any deviations from IA scattering for Q greater than 100 nm^{-1} are dominated by final-state effects, (ii) the momentum distribution $n(p)$ is expected to be Gaussian thus simplifying the analysis, (iii) the pair potential is well-known[20] and many-body contributions are expected to be small, and (iv) structural information, needed to evaluate the coefficients appearing in the Sears expansion, can therefore be computed for liquid Ne using path-integral Monte Carlo techniques.[21] The low-Q portion of the current measurements overlaps the larger wave-vector transfers achieved in the work of Buyers *et al.*,[16] while the high-Q portion is over the same Q range, with improved counting statistics, as the data of Peek *et al.* taken at $T=25.8$ K.[7]

II. DEEP-INELASTIC NEUTRON SCATTERING

A. General considerations

The double-differential scattering cross section for a system of N identical atoms is[22]

$$\frac{d^2\sigma}{d\Omega\, dE_f}=Nb^2\left[\frac{k_f}{k_i}\right]S(\mathbf{Q},\omega)\ , \tag{2}$$

where b is the bound scattering length per atom, k_i and k_f are the magnitudes of the incident and scattered neutron wave vectors, respectively, $\mathbf{Q}$ is the neutron wave-vector transfer ($\mathbf{Q}=\mathbf{k}_i-\mathbf{k}_f$), E_f is the final energy of the neutron, and $\hbar\omega$ is the energy lost by the neutron in the scattering process. $S(\mathbf{Q},\omega)$, the dynamic structure factor, can be written as[23]

$$S(\mathbf{Q},\omega)=\frac{1}{2\pi\hbar}\int_{-\infty}^{+\infty}F(\mathbf{Q},t)\exp(-i\omega t)dt\ . \tag{3}$$

The correlation function $F(\mathbf{Q},t)$ is given by

$$F(\mathbf{Q},t)=\frac{1}{N}\sum_{ij}\langle\exp[-i\mathbf{Q}\cdot\mathbf{R}_i(0)]\exp[i\mathbf{Q}\cdot\mathbf{R}_j(t)]\rangle\ , \tag{4}$$

where $\mathbf{R}_i$ and $\mathbf{R}_j$ are the atomic positions of the ith and jth atoms in the Heisenberg representation. If Q is sufficiently large then coherent processes are minimal, and in this incoherent approximation $F(\mathbf{Q},t)$ assumes the form

$$F(\mathbf{Q},t)=\frac{1}{N}\sum_{ij}\langle\exp[-i\mathbf{Q}\cdot\mathbf{R}_i(0)]\exp[i\mathbf{Q}\cdot\mathbf{R}_j(t)]\rangle\delta_{ij}\ . \tag{5}$$

If the time of passage of the neutron through the sample is short compared to the time-scale characteristic of the atomic motions in the sample then the correlation function may be approximated by its short-time behavior,[19]

$$\mathbf{R}_j(t)=\mathbf{R}_j(0)+\frac{t}{M}\mathbf{P}_j\ , \tag{6}$$

where $\mathbf{P}_j$ is the momentum of the jth atom of mass M. In this regime $S(\mathbf{Q},\omega)$ reduces to

$$S_{\mathrm{IA}}(\mathbf{Q},\omega)=\int n(\mathbf{p})\delta\left[\frac{\hbar Q^2}{2M}+\frac{\mathbf{Q}\cdot\mathbf{p}}{M}-\omega\right]d^3p\ . \tag{7}$$

This result is known as the impulse approximation. In this approximation, $S_{\mathrm{IA}}(\mathbf{Q},\omega)$ is identical to the dynamical structure factor for scattering from a noninteracting gas of atoms with momentum distribution $n(\mathbf{p})$. The argument of the δ function in Eq. (7) expresses conservation of energy and momentum for the scattering of a neutron by a single atom. In addition, the form of the argument indicates that the center of $S_{\mathrm{IA}}(\mathbf{Q},\omega)$ corresponds to the "recoil energy," Eq. (1), and its width is the result of Doppler broadening arising from the initial motion of the target atoms.

Knowledge of $n(\mathbf{p})$ permits the average single-particle kinetic energy $\langle E_k\rangle$ to be determined by integration over all particle momenta weighted by $n(\mathbf{p})$,

$$\langle E_k\rangle=\int n(\mathbf{p})\frac{p^2}{2M}d^3p\ . \tag{8}$$

In isotropic systems such as liquids, gases, and polycrystalline materials, $n(\mathbf{p})$ is also isotropic. For an isotropic Gaussian $n(p)$,

$$n(p)=\frac{1}{(2\pi\sigma_p^2)^{3/2}}\exp\left[\frac{-p^2}{2\sigma_p^2}\right]\ , \tag{9}$$

$\langle E_k\rangle$ is simply related to the width of the momentum distribution σ_p by

$$\langle E_k\rangle=\frac{3\sigma_p^2}{2M}\ . \tag{10}$$

B. y scaling

Expressing the results of the previous section in terms of the neutron Compton profile, $J(y)$, instead of $S(\mathbf{Q},\omega)$ is straightforward. When the z axis is taken to be the direction of $\mathbf{Q}$ then Eq. (7) is

$$S_{\mathrm{IA}}(\mathbf{Q},\omega)=\int n(\mathbf{p})\delta\left[\frac{\hbar Q^2}{2M}+\frac{Qp_z}{M}-\omega\right]d^3p\ , \tag{11}$$

where p_z is the z component of the target atom's momentum. With the West scaling variable y defined as[24]

$$y\equiv\left[\frac{M}{\hbar Q}\right](\omega-\omega_R)\ , \tag{12}$$

Eq. (11) can be written

$$S_{\mathrm{IA}}(\mathbf{Q},\omega)=\left[\frac{M}{\hbar Q}\right]\int\delta(\hbar y-p_z)n(\mathbf{p})d^3p\ . \tag{13}$$

Then the neutron Compton profile $J(y)$ is related to $S(\mathbf{Q},\omega)$ by

$$J(y)=\frac{\hbar^2 Q}{M}S(\mathbf{Q},\omega)\ , \tag{14}$$

and therefore

$$J_{\mathrm{IA}}(y)=\int \delta(\hbar y-p_z)n(\mathbf{p})d^3p$$
$$=\int n(p_x,p_y,\hbar y)dp_x dp_y\ , \tag{15}$$

where $J_{\mathrm{IA}}(y)$ is the function $J(y)$ in the impulse approximation.

$J_{\mathrm{IA}}(y)dy$ is the probability of finding an atom with momentum component y in the direction of $\mathbf{Q}$ in the range dy. For this reason $J_{\mathrm{IA}}(y)$ is referred to as the longitudinal momentum distribution function, the direction of $\mathbf{Q}$ defining the longitudinal direction. In an isotropic system only the magnitude of $\mathbf{Q}$ is relevant.

C. Validity of the impulse approximation

One way of determining whether the IA is valid is to discuss the scattering process in terms of classical impulsive forces. This is typically done by introducing an "interaction time" τ such that,[19]

$$Q v_0 \tau = 1\ , \tag{16}$$

where v_0 is the rms velocity of atoms in the sample and τ corresponds to the interaction time of a neutron with a target atom. In order for the IA to be valid the mean impulse delivered to the target atom by other atoms in the sample during the scattering event must be negligible compared to the momentum of the target atom, i.e.,

$$F_0\tau \ll M v_0\ , \tag{17}$$

where F_0 is the rms force acting on the target atom due to other atoms in the sample. Combining Eqs. (16) and (17) one obtains

$$\frac{F_0}{Q v_0} \ll M v_0\ . \tag{18}$$

Therefore, for the IA to be valid

$$Q \gg \frac{F_0}{2\langle E_k\rangle}\ . \tag{19}$$

This simple treatment illustrates that the regime of validity of the IA is dependent on the strength of the interatomic interactions. For liquid Ar at $T=85$ K and liquid Ne at $T=27$ K, Sears[19] calculated the ratio appearing on the right-hand side of Eq. (19). The values he determined are 34 and 47 nm^{-1} for liquid Ar and Ne, respectively. Peek determined, using a Debye model, this ratio for noble-gas solids in the neighborhood of their triple points.[25] For Ar and Ne he obtained the values of 41 and 44 nm^{-1}, respectively.

The IA is asymptotically exact for most systems as $Q\to\infty$. This has been shown to be true even for the unbounded harmonic oscillator potential.[26] For a hard-sphere fluid, however, the IA regime is never reached, not even in the limit of high Q.[27]

D. Sears expansion

The Sears expansion of the neutron Compton profile is[19]

$$J_0(y)=J_{\mathrm{IA}}(y)-A_3\left[\frac{d^3J_{\mathrm{IA}}(y)}{dy^3}\right]$$
$$+A_4\left[\frac{d^4J(y)}{dy^4}\right]-\cdots\ , \tag{20}$$

with

$$A_3=\frac{M\langle\nabla^2 V\rangle}{36\hbar^2 Q}\quad\text{and}\quad A_4=\frac{M_2\langle\mathbf{F}^2\rangle}{72\hbar^4 Q^2}\ , \tag{21}$$

where $J_0(y)$ is the observed neutron Compton profile, $J_{\mathrm{IA}}(y)$ is the longitudinal momentum distribution function, V is the interatomic potential, and $\mathbf{F}$ is the mean force on the target atom during the scattering. The terms with coefficients A_3 and A_4 are corrections to the IA arising from final-state effects, and give definite predictions for the Q dependence and the magnitude of deviations from the IA.

III. MEASUREMENT CONDITIONS

The neutron-scattering measurements were conducted on the High Resolution Medium Energy Chopper Spectrometer (HRMECS) at Argonne National Laboratory's Intense Pulsed Neutron Source (IPNS). In order to span the desired range of neutron wave-vector transfers, data were taken at four different nominal incident neutron energies: 124.6, 194.5, 299.0, and 499.1 meV. The scattered neutrons were detected in 62 ^{3}He detectors grouped in four bands located a nominal 4 m from the center of the sample. The mean scattering angles of the detector banks were 136.3°, 121.3°, 106.3°, and 87.3°. The wave-vector transfers, at these scattering angles, for the incident neutron energies employed are listed in Table I. The sample cell consisted of six 6061-T6 aluminum tubes each having an inner diameter of 0.953 cm and an outer diameter of 1.110 cm. The cell tubes were connected to a copper manifold with high-pressure tubing and positioned vertically. All sample tubes exposed 10.2 cm to the incident neutron beam.

The sample was prepared *in situ* with a clean gas-handling system by condensing 99.999% pure natural Ne obtained from the Linde Division of Union Carbide.

TABLE I. Wave-vector transfers for ^{20}Ne as a function of neutron-scattering angle for a detector bank and incident neutron energy E_i. Note: the wave-vector transfers are for ^{20}Ne.

Scattering angle ϕ (deg)	Wave-vector transfer Q (nm^{-1})			
	$E_i=124.6$ meV	194.5 meV	299.0 meV	499.1 meV
87.3	105	131	162	209
106.3	120	150	186	241
121.3	130	163	202	261
136.3	138	172	214	276

TABLE II. Properties of Ne isotopes.

Isotope	Abundance (%)[a]	Mass (amu)[a]	σ_s[b] (b)	Scattering intensity (%)
^{20}Ne	90.51	19.992	2.671	92.76
^{21}Ne	0.27	20.994	5.7	0.59
^{22}Ne	9.22	21.991	1.88	6.65

[a]Data taken from F. W. Walker, D. G. Miller, and F. Feiner, *Chart of the Nuclides* 13th ed. (General Electric Company, San Jose, 1983).

[b]Scattering cross-section data taken from V. F. Sears, in *Methods of Experimental Physics,* edited by D. L. Price and K. Sköld (Academic, Orlando, 1986), Vol. 23A, p. 534.

There are three stable isotopes of Ne. Their relative natural abundances and neutron-scattering properties are listed in Table II, which indicates that the vast majority of neutrons scattered by a natural Ne sample are scattered by ^{20}Ne. The presence of ^{22}Ne was taken into account as discussed in Sec. IV B.

The cell temperature during the experiment was maintained by a Displex closed-cycle refrigeration system. Si diode thermometers, located at the top and the bottom of the cell assembly, were used to record the cell temperatures periodically. The temperature difference across the assembly was approximately 1.4°, but the temperature difference across the liquid Ne was certainly less than this. Temperature variations, defined to be the standard deviation of the recorded temperatures, were approximately 0.1°. The stated sample temperature of 27 K is the average of the temperatures recorded by the two thermometers. The sample pressure was approximately 0.7 MPa. At 27 K this corresponds to a Ne sample density of 36.1 atoms nm^{-3}.[28]

At each incident-neutron energy a filled cell and empty cell data set were taken. Data collection at each incident energy took approximately 48 h, half this time being spent collecting data from the filled cell, the other half from the empty cell.

IV. DATA ANALYSIS

The purpose of this work is to go beyond a mere consistency check between the scattering data and a theory for final-state effects. To do this, the key parameter, wave-vector transfer Q, needs to be varied over a wide range. In addition, the important effects of instrument resolution and multiple scattering on the measured neutron Compton profiles need to be well understood and accounted for. In this section we demonstrate how one corrects for such effects and that a quantitative measurement of final-state effects emerges unambiguously from the analysis.

A. Scattering corrections and instrument simulation

The primary correction to the filled sample cell time-of-flight data is the subtraction of the empty cell scattering. Because the scattering from the liquid Ne and the scattering from the Al cell have significant overlap, good counting statistics are necessary in both the filled cell and empty cell runs. For our Ne samples, at the three lower incident neutron energies, obtaining a high-quality empty cell run was particularly important due to the presence of diffraction peaks in the time-of-flight spectra. These diffraction peaks were due to coherent scattering from the Al tubes and from an unshielded Cu manifold which although not in the direct neutron beam contributed noticeable intensity to the time-of-flight spectra due to the poor vertical collimation of the neutron pulses.

The empty cell run and the filled cell run were not of exactly the same duration, nor was the incident neutron flux constant in time; therefore the empty cell data were scaled for each run using a scaling factor determined from the integrated neutron intensity from a beam monitor, located before the sample assembly. In addition, the incident neutron energy for the empty cell run tended to vary slightly from that for the filled cell run (typically by less than 1 meV). This energy difference shifts the filled cell and empty cell time-of-flight spectra relative to one another (by less than 1 μs). To correct for this a program was written which calculated the time-of-flight for a neutron inelastically scattered from Al, in the IA, for the incident neutron energies characteristic of the filled and empty cell runs. The empty cell time-of-flight data were then shifted by the difference in these calculated times-of-flight before being subtracted from the filled cell data.[29]

For analysis of these Ne data we used a sophisticated Monte Carlo chopper-spectrometer simulation program, SPEC_SIM, developed by Blasdell.[30,31] This program generates both a function which tells how the scattering is modified by finite instrument resolution and the sample-dependent multiple-scattering corrections. In order to determine the instrument resolution function it is necessary (i) to characterize the time and velocity distribution of the neutron pulse emerging from the face of the moderator,[32] and (ii) to determine the average chopper open-time, the effective width of the moderator, and the source emission time delay. This determination is done in SPEC_SIM by fitting the time spectra recorded by the two BF_3 beam monitors, accounting quantitatively for the neutron beam chopping as well as for the response of the monitors.

Given the pulse-shape parameters, SPEC_SIM performs a Monte Carlo simulation in order to calculate the instrument resolution function. This is done by simulating the scattering of neutrons, in the IA, from a Ne sample with nuclei which are fixed before the scattering event. The sample, sample cell, and instrument materials and geometry used in the simulation are the same as those in the actual experiment. The calculation therefore includes the effects of sample attenuation on the multiple scattering and upon the instrument resolution. In this case, any broadening of the (y-scaled) simulation singly scattered neutron time-of-flight data is due to instrument resolution. The Ne cross-section-weighted mass of 20.1368 amu was used in the simulation and in the y scaling of the measured time-of-flight data.

The instrument resolution functions generated for the

experimental conditions identical to those of our liquid Ne sample for the 136.3° detector bank are shown in Fig. 1 and Table I. Table III lists the standard deviations for all the instrument resolution functions employed. It should be noted that (i) the resolution functions are asymmetric in y, and (ii) the width of the resolution functions increases with increasing incident neutron energy. This same behavior is seen in the resolution functions generated using the analytical formalism of Loong, Ikeda, and Carpenter[33] which, unlike SPEC_SIM, does not take into account the effect of finite sample size. The widths, as measured by the standard deviation, of the resolution functions for the 87.3° detector bank are essentially the same for a point scatterer and for a scatterer having the physical dimensions of our sample. For the 136.3° detector bank however, the width of the resolution functions for our sample geometry are larger than those for a point scatterer by as much as 17%.

For the present data SPEC_SIM predicts that 9% of the total scattering, after the empty cell scattering has been subtracted, was due to sample-dependent multiple scattering. Such scattering is primarily due to neutrons that scatter twice from Ne atoms or once from the Al cell and once from a Ne atom. Figure 2 shows the relative sizes of the various backgrounds for data converted to $J(y)$. We note that the shape of the multiple-scattering contribution calculated using SPEC_SIM is very different than the shape of the low-order polynomial background used to account for multiple scattering in the earlier $n(p)$ measurements on liquid Ne by Peek *et al.*[7]

B. Extraction of the model parameters

Once the simulation sample-dependent multiple scattering contribution has been subtracted from the observed spectra, the data are fit by numerically convoluting a model response, whose parameters are varied to obtain the "best" fit with the observed data, with the instrument resolution function

$$J_0(y)=\int_{y_{\min}}^{y_{\max}} R(y-y')J_m(y')dy'+F(y) . \quad (22)$$

Here $J_0(y)$ is the measured neutron Compton profile, $R(y-y')$ is the instrument resolution function, and $J_m(y')$ is the model neutron Compton profile, and $F(y)$ is a second-order polynomial which allows for sample-dependent multiple scattering not accounted for by the

TABLE III. Standard deviations for the instrument resolution functions generated by SPEC_SIM. The wave-vector transfers are for ^{20}Ne. See Text Sec. IV A.

Scattering angle ϕ (degrees)	Q (nm^{-1})	Standard deviation (nm^{-1})
	E_i=124.6 meV	
87.3	105	1.14
106.3	120	1.00
121.3	130	0.97
136.3	138	0.97
	E_i=194.5 meV	
87.3	131	1.48
106.3	150	1.30
121.3	163	1.24
136.3	172	1.24
	E_i=299.0 meV	
87.3	162	1.99
106.3	186	1.75
121.3	202	1.66
136.3	214	1.65
	E_i=499.1 meV	
87.3	209	3.11
106.3	241	2.72
121.3	261	2.56
136.3	276	2.51

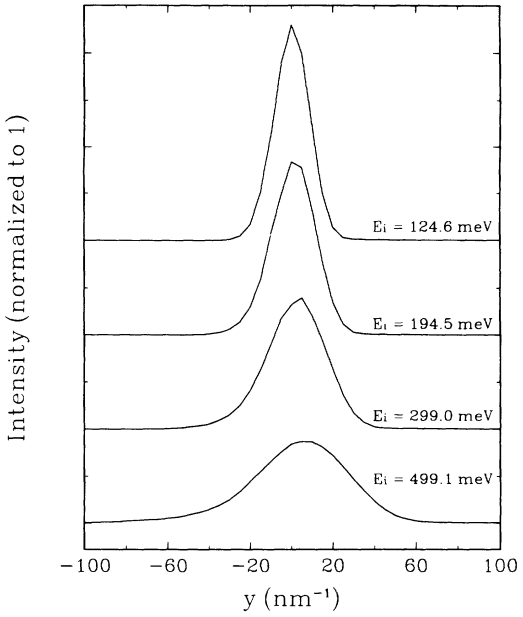

FIG. 1. Chopper-spectrometer resolution functions calculated for scattering from the liquid Ne sample into the spectrometer 136.3° detector bank, for four incident neutron energies used in the present work.

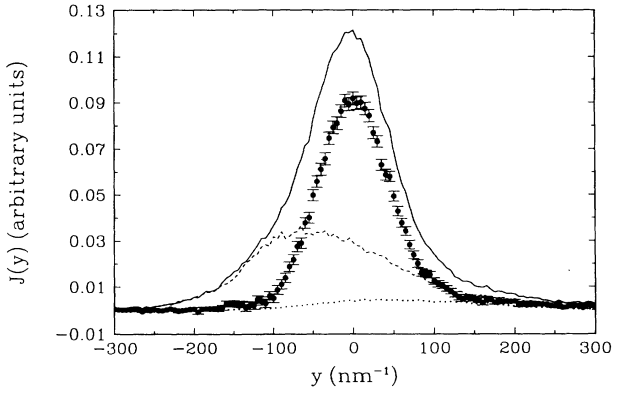

FIG. 2. y-scaled background subtraction and multiple-scattering corrections for $\langle\phi\rangle$=106.3°, E_i=499.1 meV: filled-sample-cell time-of-flight data (solid line); empty cell data (dashed line); data difference (solid circles with error bars); sample-dependent multiple scattering calculated with SPEC_SIM (dotted line).

simulation.[34] The contribution of $F(y)$ was very small, amounting typically to only a percent of the peak intensity. In Eq. (22) the limits of integration, $y_{\min}$ and $y_{\max}$, were -250 and $+250$ nm^{-1}, respectively. The "best" fit is taken to be the one with the smallest reduced χ^2.

C. Identification of the final-state contribution of the scattering

The model response represents the neutron Compton profile that would be observed if the instrument resolution function were a δ function. It was composed of two functions, each having the form of the first two terms in the Sears expansion,

$$J_m(y)=\sum_{i=1}^{2} J_{\mathrm{IA}}^{(i)}(y)-A_3^{(i)}\frac{d^3 J_{\mathrm{IA}}^{(i)}(y)}{dy^3} , \tag{23}$$

where

$$A_3^{(i)}=\frac{M_i\langle \nabla^2 V\rangle}{36\hbar Q_i} , \tag{24}$$

and

$$J_{\mathrm{IA}}^{(i)}(y)=\frac{B_i}{(2\pi\sigma_{(i)}^2)^{3/2}}\exp\left[\frac{(y-y_0^{(i)})^2}{2\sigma_{(i)}^2}\right] . \tag{25}$$

The index i refers to the relevant Ne isotope ($i=1$ for ^{20}Ne and $i=2$ for ^{22}Ne). The pair potential $V(r)$ is assumed to be identical for ^{20}Ne and ^{22}Ne.

The respective $J_{\mathrm{IA}}(y)$, of the Ne isotopes appearing in Eq. (23) are assumed to be Gaussian. In nonclassical liquids, to order $\hbar^2$ in a Wigner-Kirkwood expansion, the momentum distribution remains Gaussian.[35] Furthermore, measurements of $n(p)$ in liquid Ne at $T=25.8$ K density 36.3 atoms nm^{-3} (close to our sample temperature and density) found no indication of non-Gaussian behavior within their experimental accuracy.[7]

Appropriate parameters appearing in Eqs. (23)–(25) were constrained in order to reduce the number of free parameters in the fits. The widths, σ [see Eq. (9)], of the $J_{\mathrm{IA}}(y)$ were determined by assuming that $\langle E_k\rangle$ is given by

$$\langle E_k\rangle=\frac{3}{2}k_B T_{\mathrm{eff}} , \tag{26}$$

with

$$T_{\mathrm{eff}}=T\left\{1+\frac{1}{12}\left[\frac{\theta}{T}\right]^2-\frac{1}{240}\left[\frac{\theta}{T}\right]^4+\cdots\right\} , \tag{27}$$

and

$$\theta^2=\frac{\hbar^2\langle \nabla^2 V(r)\rangle}{3Mk_B} , \tag{28}$$

where T is the physical sample temperature (27 K), V is the pair-potential energy, M is the mass of the atom, and $\langle\cdots\rangle$ denotes a thermal average. The term of order $\hbar^2$ in Eq. (27) is exact while the term of order $\hbar^4$ is an approximate result obtained under the assumption that the spectral density of the velocity autocorrelation function is Gaussian.[36]

A good estimate of $\langle E_k\rangle$ can be obtained using the accurate pair potential for Ne developed by Aziz, Meath, and Allnatt[37] and $g(r)$, the radial distribution function. The average of the Laplacian of the potential energy is formally

$$\langle \nabla^2 V(r)\rangle=4\pi\rho\int \nabla^2 V(r) g(r) r^2 dr , \tag{29}$$

where ρ is the sample density. $g(r)$ has not been measured for liquid Ne at the temperature and density of our sample, therefore a $g(r)$ calculated using path-integral Monte Carlo techniques (PIMC) was used.[38] Use of this $g(r)$ and the HFD-C2 potential[37] yields a value of 52.4 K for θ.

In the calculation of $\langle E_k\rangle$ of ^{20}Ne and ^{22}Ne it was assumed that $\langle \nabla^2 V(r)\rangle$ is the same for both isotopes. Because T_{eff}, the effective temperature, is mass dependent, [see Eqs. (27) and (28)], $\langle E_k(^{20}\mathrm{Ne})\rangle$ is 1.5% larger than $\langle E_k(^{22}\mathrm{Ne})\rangle$ at 27 K. For ^{20}Ne at this temperature and sample density $T_{\mathrm{eff}}=33.9$ K, so $\langle E_k\rangle=50.9$ K. A recent PIMC calculation[21] of $\langle E_k\rangle$ in liquid ^{20}Ne at $T=27$ K yielded a value of 51.3 ± 0.4 K, which is consistent with our Wigner-Kirkwood expansion result.

In the fitting process the scattering intensity B_2 of ^{22}Ne was constrained to be 7.2% of B_1, the intensity of ^{20}Ne (Table II). In addition, the distance between the centers of $J_{\mathrm{IA}}(y)$ for the two isotopes was held fixed at a value determined by the scattering kinematics. Due to uncertainty in the y scale, arising from the determination of mean incident-neutron energy and uncertainties in the sample and instrument geometry, the absolute positions of the scattering peaks in y were *not* held fixed.

The neutron Compton profile for a natural Ne sample will have an antisymmetric component even in the absence of final-state effects. This is because the scattering from ^{20}Ne is kinematically separate from that from ^{22}Ne, due to the difference in their masses. We note that the size of the largest correction to the IA is determined by the A_3 term in the Sears expansion, a term which is antisymmetric in y. As Q increases, the separation between the ^{20}Ne and ^{22}Ne responses increases. At very large Q, where the IA is expected to be valid, the size of the antisymmetric component in the observed profile arising from the kinematic separation of the scattering can be significant. Note that the polarity of the antisymmetric component due to the kinematic separation of the scattering is *opposite* to that of the A_3 term in the Sears expansion. At the Q's employed in the present work, however, this effect is very small and is removed by using a model response of the form given in Eq. (23).

As mentioned previously, the raw time-of-flight data were y scaled using the cross-section-weighted mass of 20.1368 amu. Changes in the width and position of the IA component of the response brought about by this choice of a y-scaling mass were corrected using a method described elsewhere.[39]

V. RESULTS AND DISCUSSION

A. Results and conclusions for liquid Ne

By fitting the observed neutron Compton profiles with a model having the form of Eq. (23), values for A_3 were obtained for liquid Ne for Q's in the range 105 to 276 nm^{-1}. For all fits, χ^2 values are listed in Table IV and corresponding values for A_3 are listed in Table V.[40] In general the fits to the data using the model response of Eq. (23) are very good.

Typical fits to the data are shown in Figs. 3–6. The dotted line in each of these figures is the polynomial background $F(y)$ in Eq. (22). The fit residuals are the difference between the data and the fit, divided by the uncertainty associated with the data. Note that the residuals are very evenly distributed over the entire profile, with no systematic deviations evident.

Additional fits using a model function which included the A_4 term yielded A_4 coefficients with very large uncertainties and no discernible Q dependence. It is important to note that inclusion of the A_4 term did not appreciably change the values of the A_3 coefficients obtained from fits that did *not* include the A_4 term. This increases confidence in the identification of the A_3 magnitudes. The A_4 term is most likely not detectable in the present data due to its small size and symmetry, which is the same symmetry as the IA component of Sears' expansion.

The A_3 coefficients versus Q are plotted in Fig. 7. Also shown in Fig. 7 is a line showing A_3 computed using Eq. (21). The average of the Laplacian appearing in Eq. (24), $\langle \nabla^2 V \rangle$, was calculated using (a) the same PIMC-generated $g(r)$ used to compute the effective temperature (Sect. IV C), because no measured $g(r)$ is available, and (b) the same Ne-Ne pair potential of Aziz and Chen.[20] The value of this $\langle \nabla^2 V \rangle$ is given in Table VI as the entry for 26.1-K liquid. Figure 7 shows that both (i) the Q dependence of the A_3 coefficient is in good agreement with the Q^{-1} behavior predicted by Sears' theory, and (ii) the magnitude of the A_3 coefficient as a function of Q is in good agreement with expectations.

One may ask, how large are expected final-state effects for other Ne liquids, and how are they expected to depend upon density at a fixed temperature? As examples, we therefore include in Table VI values of $\langle \nabla^2 V \rangle$ calculated for a series of three Ne liquids at 35 K, for which measured $S(Q)$'s are available.[41] In these cases, we calculated a $g(r)$ corresponding to the tabulated $S(Q)$, then used this $g(r)$ in the $\langle \nabla^2 V \rangle$ calculation with the Aziz potential.[20] One sees that the final-state effects increase with increasing density of the liquid. This can be understood by examining the numerical details of the calculation of $\langle \nabla^2 V \rangle$. The magnitude of $r^2 \langle \nabla^2 V \rangle$ falls steeply with increasing r, and is largest for r below 0.27 nm. It is below approximately this value of r that $g(r)$ increases as

TABLE IV. χ^2 for fits to liquid Ne data for 95 degrees of freedom.

Scattering angle ϕ (degrees)	χ^2 Incident neutron energy (meV) 124.6	194.5	299.0	499.1
87.3	123	103	83	73
106.3	66	102	119	63
121.3		134	84	69
136.3	151	129	116	76

TABLE V. Values for the A_3 coefficient for liquid ^{20}Ne, determined from the fits, as a function of scattering angle and incident neutron energy E_i.

Scattering angle ϕ (degrees)	Q (nm^{-1})	A_3 (nm^{-3})
	$E_i = 124.6$ meV	
87.3	105	3380±210
106.3	120	2990±240
136.3	138	2700±240
	$E_i = 194.5$ meV	
87.3	131	2100±300
106.3	150	2500±400
121.3	163	3200±400
136.3	172	2700±400
	$E_i = 299.0$ meV	
87.3	162	1900±400
106.3	186	2300±400
121.3	202	2500±400
136.3	214	1800±400
	$E_i = 499.1$ meV	
87.3	209	1500±500
106.3	241	2000±500
121.3	261	700±500
136.3	276	1000±500

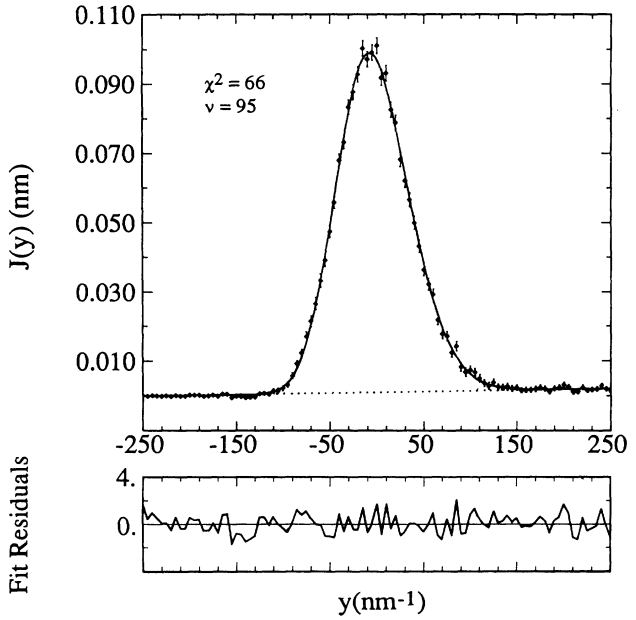

FIG. 3. Neutron Compton profile, data and fit for $E_i = 124.6$ meV ($\langle \phi \rangle = 106.3°$, $\langle Q \rangle = 121$ nm^{-1}). The fitting procedure is detailed in the text Sec. V. The dotted line is the term $F(y)$ in Eq. (22). The fit residuals are the difference between the data and the fit, divided by the uncertainty associated with the data. χ^2 is the chi-squared value for the fit, ν is the number of degrees of freedom.

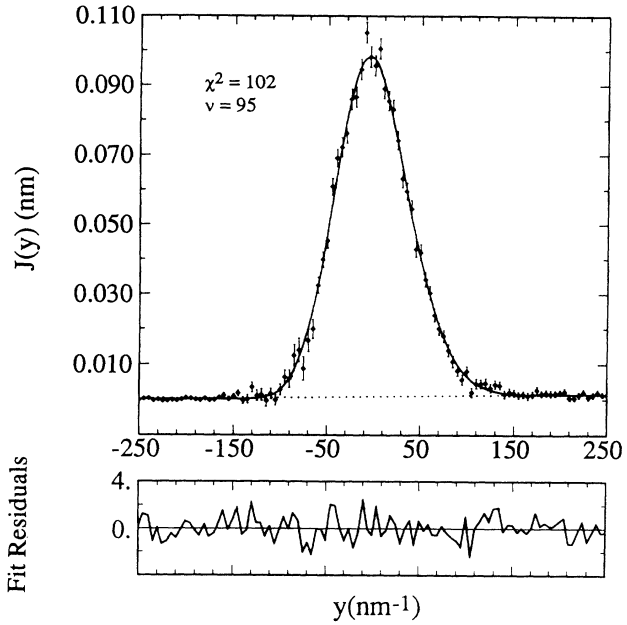

FIG. 4. Data and fit for $E_i = 194.5$ meV ($\langle\phi\rangle = 106.3°$, $\langle Q\rangle = 150\ \text{nm}^{-1}$). Other matters are as for Fig. 3. Note that the residuals are evenly distributed over the range of wave-vector transfers y.

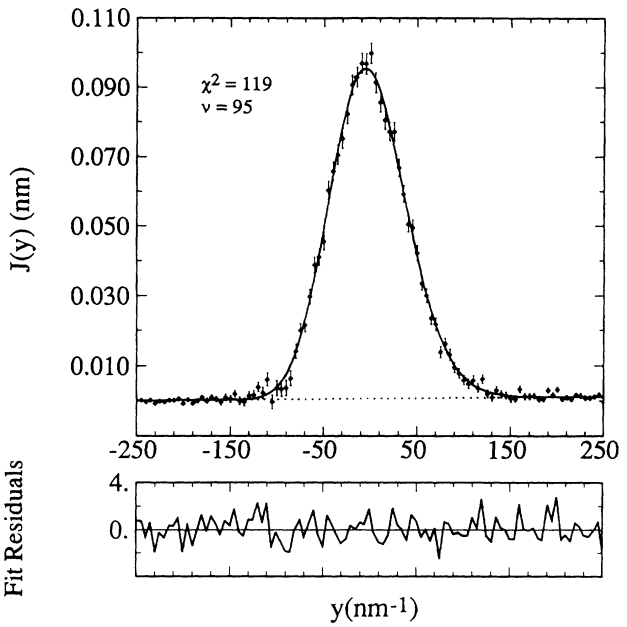

FIG. 5. Data and fit for $E_i = 299.0$ meV ($\langle\phi\rangle = 106.3°$, $\langle q\rangle = 186\ \text{nm}^{-1}$).

density increases, although the position of the first peak in $g(r)$ remains at approximately 0.305 nm, essentially unchanged with change of liquid density.

Another value of $\langle \nabla^2 V\rangle$ in Table VI deserves comment: that for 35 K and 33.4 atoms nm^{-3}. It comes from a PIMC calculation of $g(r)$ using the Aziz pair potential.[20] The result differs somewhat from that which uses a $g(r)$ derived from experiment,[42] but the difference is not large enough to alter the key conclusions (i) and (ii) above.

Finally, in order to indicate more explicitly the relative size of the contribution arising from the A_3 term for ^{20}Ne at 26.1 K and 36.4 atoms nm^{-3}, Figs. 8 and 9 show the IA contribution (symmetric in y) and the antisymmetric A_3 contribution, determined from the data fits, for the largest and smallest Q's examined.

TABLE VI. Values of the average Laplacian, Eq. (29), for condensed ^{20}Ne, calculated using the pair potential of Ref. 20. A larger value indicates a larger antisymmetric final-state effect on the deep-inelastic neutron scattering at a given Q.

Phase	Density (atoms nm^{-3})	Temperature (K)	$10^{-2}\langle\nabla^2 V(r)\rangle$ (K nm^{-2})
Liquid[a]	36.1	27.8	3426
Liquid[b]	34.7	35	3498
Liquid[b]	33.4	35	3157
Liquid[b]	31.7	35	3092
Liquid[a]	33.4	35	2915
Solid[a]	44.97[c]	4.2	4362
Solid[a]	44.85[c]	10.0	4377
Solid[a]	43.78[c]	20.0	4441

[a]Ref. 21, $g(r)$ calculated by PIMC simulation.
[b]Ref. 41, measured $S(Q)$ converted to $g(r)$.
[c]D. N. Batchelder, D. L. Losee, and R. O. Simmons, Phys. Rev. **162**, 767 (1967).

B. Expectations about final-state effects in solid Ne

The average Laplacian appearing in A_3, Eq. (21), can be calculated for the solid phase as well, provided a suitable angle-averaged $g(r)$ is available for the integral, Eq. (29). The resulting values my be applied to measurements on polycrystalline solids. Such $g(r)$'s have been calculat-

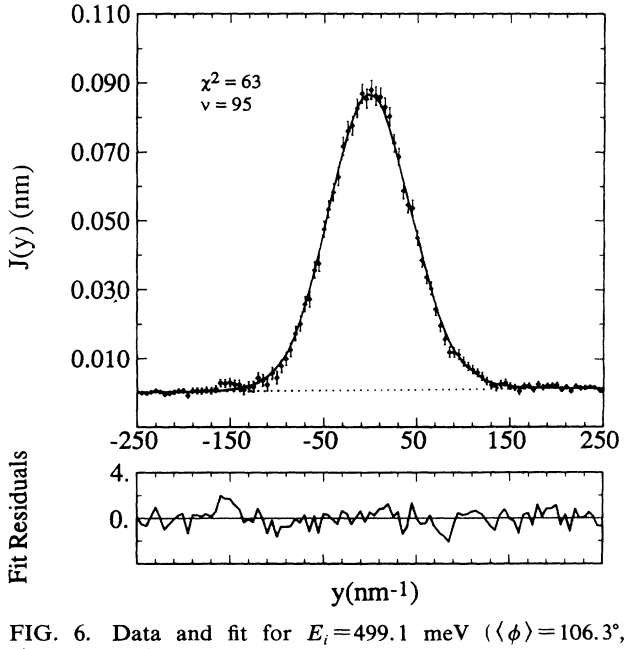

FIG. 6. Data and fit for $E_i = 499.1$ meV ($\langle\phi\rangle = 106.3°$, $\langle Q\rangle = 241\ \text{nm}^{-1}$).

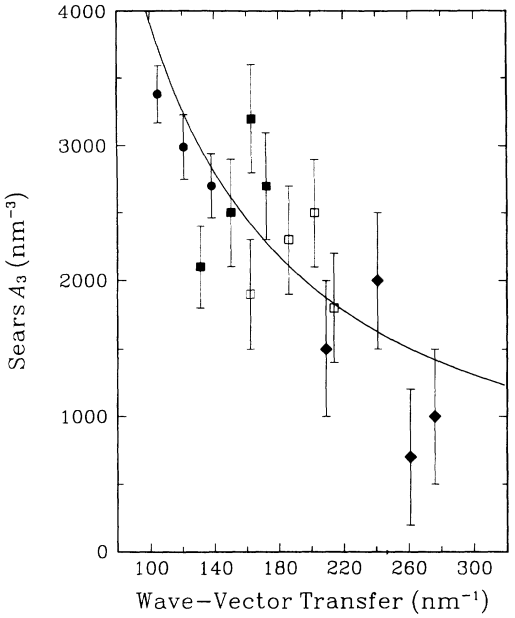

FIG. 7. First antisymmetric coefficients, A_3, versus wave-vector transfer Q, for liquid ^{20}Ne at 27 K. For each incident neutron energy, a range of Q's is measured by the range of detector banks: $E_i=124.6$ meV (solid circles); $E_i=194.5$ meV (solid squares); $E_i=299.0$ meV (open squares); $E_i=499.1$ meV (solid diamonds). The solid line is calculated as described in Sec. V A. There is very good agreement between the measurements and the calculation for both the Q dependence and magnitude of A_3.

ed by PIMC simulation,[21] with the same pair potential[20] employed for the liquid calculations used in the present work. The corresponding values of $\langle \nabla^2 V \rangle$ are also collected in Table VI.

For the solids, a small increase in $\langle \nabla^2 V(r) \rangle$ with increasing temperature is shown in Table VI. In detail, this

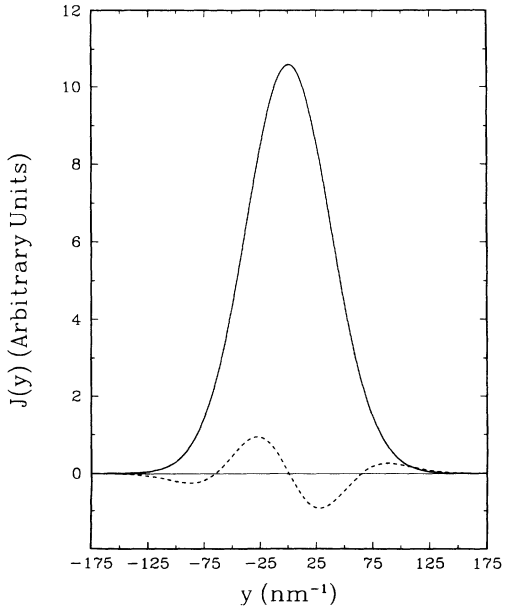

FIG. 8. The IA component (solid line) and first antisymmetric component (dashed line) as determined from the fit to the $E_i=124.6$ meV, $\langle \phi \rangle=87.3°$, $\langle Q \rangle=104$ nm^{-1} data.

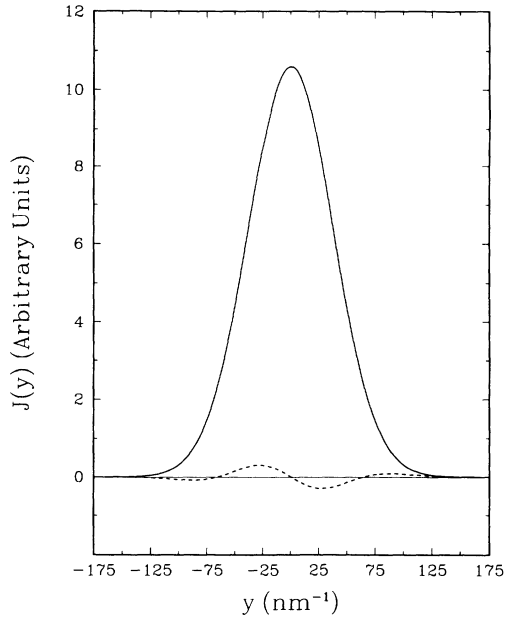

FIG. 9. The IA component (solid line) and first antisymmetric component (dashed line) as determined from the fit to the $E_i=499.1$ meV, $\langle \phi \rangle=136.3°$, $\langle Q \rangle=277$ nm^{-1} data.

arises because the amplitude of thermal motion in the lattice increases with increasing temperature, and the first maximum in $g(r)$ broadens slightly. This includes more overlap with the second derivative of the repulsive part of the potential, in the crucial region below $r=0.27$ nm. The repulsive part of the potential contributes about 93% to each calculated average. The contrary effect of density decrease owing to thermal expansion is much smaller, so that in the case of equilibrium density solid Ne, the larger final-state effect in scattering is expected for the less-dense solid at higher temperature.

VI. CONCLUSION

We conclude that Sears' theory provides a quantitatively accurate description of final-state effects in liquid Ne. This is a quantitative demonstration of final-state effects in a condensed system other than ^{4}He.

To permit a more precise determination of A_3 and possibly allow A_4 to be extracted, future experiments on liquid Ne would require increased counting statistics, a thinner-walled incoherent-scattering cell, and probably a more fully shielded spectrometer[34] to permit a totally complete Monte Carlo simulation of sample-dependent and other scattering.

ACKNOWLEDGMENTS

We thank R. C. Blasdell for advice in the use of data reduction software. We are much indebted to M. Boninsegni and D. M. Ceperley for the PIMC calculations of Ref. 21 used in our data analysis. This research was sup-

ported by the U.S. Department of Energy, BES-Materials Sciences under Contract No. DE-FG02-91ER45439. It has benefited from the use of the Intense Pulsed Neutron Source (IPNS) at Argonne National Laboratory. We are pleased to acknowledge the able assistance of the staff of this facility, funded by the U.S. Department of Energy, BES-Materials Sciences, under contract No. W-31-109-ENG-38.

*Present address: Department of Physics and Astronomy, Colgate University, 13 Oak Drive, Hamilton, NY 13346-1398.

[1]R. O. Hilleke, P. Chaddah, R. O. Simmons, D. L. Price, and S. K. Sinha, Phys. Rev. Lett. **52**, 847 (1984); R. O. Simmons, Can. J. Phys. **65**, 1401 (1987).

[2]R. C. Blasdell, D. M. Ceperley, and R. O. Simmons, Z. Naturforsch. **48a**, 433 (1993).

[3]V. F. Sears, E. C. Svensson, P. Martel, and A. D. B. Woods, Phys. Rev. Lett. **49**, 279 (1982); H. Mook, Phys. Rev. B **37**, 5806 (1988); W. M. Snow, Y. Wang, and P. E. Sokol, Europhys. Lett. **19**, 403 (1992).

[4]K. H. Andersen, W. G. Stirling, A. D. Taylor, S. M. Bennington, Z. A. Bowden, I. Bailey, and H. R. Glyde, Physica B **181**, 865 (1992).

[5]V. F. Sears, Can. J. Phys. **59**, 555 (1981).

[6]D. A. Peek and R. O. Simmons, J. Chem. Phys. **94**, 3169 (1990); D. A. Peek, I. Fujita, M. C. Schmidt, and R. O. Simmons, Phys. Rev. B **45**, 9680 (1992); M. A. Fradkin, S.-X. Zeng, and R. O. Simmons, *ibid.* **49**, 3197 (1994).

[7]D. A. Peek, M. C. Schmidt, I. Fujita, and R. O. Simmons, Phys. Rev. B **45**, 9671 (1992).

[8]W. E. Langel, D. L. Price, R. O. Simmons, and P. E. Sokol, Phys. Rev. B **38**, 275 (1988); K. W. Herwig, J. C. Gavilano, M. C. Schmidt, and R. O. Simmons, *ibid.* **41**, 96 (1990); J. Mayers, Phys. Rev. Lett. **71**, 1553 (1993).

[9]R. Hempelmann, D. Richter, and D. L. Price, Phys. Rev. Lett. **58**, 1016 (1987); R. Hempelmann, D. L. Price, G. Reiter, and D. Richter, in *Momentum Distributions,* edited by R. N. Silver and P. E. Sokol (Plenum, New York, 1989), p. 213; K. W. Herwig and R. O. Simmons, *ibid.*, p. 203.

[10]P. Postorino, F. Fillaux, J. Mayers, J. Tomkinson, and R. S. Holt, J. Chem. Phys. **94**, 4411 (1991).

[11]M. P. Paoli and R. S. Holt, J. Phys. C **21**, 3633 (1988).

[12]P. Verkerk, P. H. K. de Jong, M. Arai, S. M. Bennington, W. S. Howells, and A. D. Taylor, Physica B **181**, 824 (1992); A. C. Evans, J. Mayers, D. N. Timms, and M. J. Cooper, Z. Naturforsch. **48a**, 425 (1993).

[13]See, for example, numerous papers in *Momentum Distributions,* edited by R. N. Silver and P. E. Sokol (Plenum, New York, 1989), and references therein.

[14]A preliminary report of some of this work, without analysis, appeared in M. A. Fradkin, S.-X. Zeng, and R. O. Simmons, Z. Naturforsch. **48a**, 438 (1993).

[15]See, for example, S. H. Chen, O. J. Eder, P. A. Egelstaff, B. C. G. Haywood, and F. J. Webb, Phys. Lett. **19**, 269 (1965).

[16]W. J. L. Buyers, V. F. Sears, P. A. Lonngi, and D. A. Lonngi, Phys. Rev. A **11**, 697 (1967).

[17]C. Carraro and S. E. Koonin, Phys. Rev. Lett. **65**, 2792 (1990); A. Belić and V. R. Pandharipande, Phys. Rev. B **45**, 839 (1992).

[18]R. N. Silver, Phys. Rev. B **37**, 3794 (1988); **38**, 2283 (1988); **39**, 4022 (1989).

[19]V. F. Sears, Phys. Rev. B **30**, 44 (1984).

[20]R. A. Aziz and H. H. Chen, J. Chem. Phys. **67**, 5719 (1977). See, also, R. A. Aziz, in *Inert Gases: Potentials, Dynamics and Energy Transfer in Doped Crystals,* edited by M. L. Klein (Springer-Verlag, Berlin, 1984).

[21]D. N. Timms, M. Boninsegni, D. M. Ceperley, A. C. Evans, J. Mayers, and R. O. Simmons (unpublished).

[22]L. Van Hove, Phys. Rev. **95**, 249 (1954).

[23]V. F. Sears, Phys. Rev. B **30**, 44 (1984).

[24]G. B. West, Phys. Rep. **18C**, 263 (1975).

[25]D. A. Peek, Ph.D. thesis, University of Illinois at Urbana-Champaign, 1989.

[26]J. M. F. Gunn and M. Warner, Z. Phys. B **56**, 13 (1984).

[27]J. J. Weinstein and J. W. Negele, Phys. Rev. Lett. **49**, 1016 (1982).

[28]R. M. Gibbons, Cryogenics **9**, 251 (1969).

[29]Because of approximately 4% attenuation of the neutron pulse by the liquid Ne, slightly more neutrons scatter from the rear of the Al cell in the empty cell run than in the filled cell run. Because of practical uncertainties in the angle dependence of this attenuation effect and its magnitude being substantially smaller than the sample-dependent multiple-scattering correction, this effect was ignored in the raw data subtraction of cell background data.

[30]R. C. Blasdell, Ph.D. thesis, University of Illinois at Urbana-Champaign, 1992. There are several programs in the simulation package, but for convenience they will all be referred to here as SPEC_SIM.

[31]R. C. Blasdell and J. M. Carpenter (unpublished).

[32]SPEC_SIM assumes the emission time distribution of the neutron pulse at the moderator face is given by the semiempirical function of S. Ikeda and J. M. Carpenter [Nucl. Instrum. Meth. Phys. Res. Sect. A **239**, 536 (1985)]. This function has been found to fit very well the time structure of neutron pulses from the IPNS liquid methane moderators over a wide neutron energy range. [C.-K. Loong, S. Ikeda, and J. M. Carpenter, Nucl. Instrum. Meth. Phys. Res. Sect. A **260**, 381 (1987).]

[33]See Ref. 32.

[34]Sample-dependent multiple scattering from an unknown source, possibly from a poorly shielded component in the final flight path, requires the use of a polynomial background function in the analysis of all deep-inelastic-scattering experiments on HRMECS. See also Ref. 30.

[35]L. D. Landau and E. M. Lifshitz, *Statistical Physics,* 3rd ed. (Pergamon, New York, 1980), p. 104. Also see, for example, F. Barocchi, M. Neumann, and M. Zoppi, Phys. Rev. A **36**, 2440 (1987), and references contained within.

[36]V. F. Sears, Phys. Rev. A **7**, 340 (1973).

[37]R. A. Aziz, W. J. Meath, and A. R. Allnatt, Chem. Phys. **78**, 295 (1983).

[38]D. M. Ceperley and M. Boninsegni (private communication).

[39]M. A. Fradkin, Ph.D. thesis, University of Illinois at Urbana-Champaign, 1993.

[40]Due to the presence of an extremely large diffraction peak in the $Q=131$ nm^{-1}, $E_i=124.6$ meV time-of-flight data that was not cleanly removed by the subtraction of the empty cell scattering, this data set was not analyzed.

[41]L. A. de Graaf and B. Mozer, J. Chem. Phys. **55**, 4967 (1971).

[42]We note that the PIMC and experimentally derived $g(r)$'s are very similar, but differ essentially only by being displaced slightly in r, the PIMC $g(r)$ lying at smaller r.